Available online at www.sciencedirect.com
ScienceDirect
Journal of Catalysis 254 (2008) 71–78
JOURNAL OF CATALYSIS
www.elsevier.com/locate/jcat

Hydrogenation of crotonaldehyde on different Au/CeO_2 catalysts

Betiana Campo [a], Corinne Petit [b], María A. Volpe [a,*]

[a] *PLAPIQUI, Camino Carrindanga km 7, 8000 Bahía Blanca, Argentina*
[b] *LMSPC, UMR 7515 du CNRS, ECPM, ULP, 25, rue Becquerel, 67087 Strasbourg Cedex 2, France*

Received 9 October 2007; revised 28 November 2007; accepted 28 November 2007

Available online 16 January 2008

Abstract

The gas-phase hydrogenation of crotonaldehyde was carried out at 120, 150, and 180 °C over Au catalysts supported on ceria with low and medium surface areas (150 and 80 $m^2\,g^{-1}$, respectively). An initial deactivation period was observed, followed by a steady-state regime. Ethanol was the main product in the deactivation period, whereas crotyl alcohol, butanal, butanol, and condensation products were produced under steady-state conditions. The activity and selectivity to crotyl alcohol (in the 20–32% range) were lower than those for the high-surface area ceria catalysts studied previously [B. Campo, M. Volpe, S. Ivanova, R. Touroude, J. Catal. 242 (2006) 162]. Samples were characterized by TPR, XPS, TEM, and XRD. The analysis of catalytic and characterization results indicates that gold particles supported on low- and medium-surface area ceria were relatively large, and the promotional effect of Ce^{3+} species was not achieved for the corresponding catalysts. Moreover, under reductive conditions, sintering still increased gold particle size.

Keywords: Gold; Ceria; Crotonaldehyde hydrogenation; Selective hydrogenation

1. Introduction

The hydrogenation of a carbonyl bond in a molecule that also contains a C=C double bond (as in α,β-unsaturated compounds) is extremely difficult. Thermodynamics favors the hydrogenation of the C=C bond over the C=O bond by about 35 kJ/mol [1]; moreover, for kinetic reasons, the reactivity of the C=C bond is greater than that of the C=O bond. Conventional hydrogenation catalysts based on Pt, Ru, Ni, and Pd produce mainly saturated aldehyde. The development of new catalysts able to selectively hydrogenate the carbonyl group is important both from a fundamental standpoint and for the eventual synthesis of speciality chemicals. In this context, gold catalysts have been studied.

Several research groups have reported that gold-supported catalysts show a remarkable selectivity toward the hydrogenation of the conjugated C=O bond in the hydrogenation of α,β-unsaturated compounds [2–10]. These results demonstrate that a peculiarity of gold is its intrinsic selectivity toward hydrogenation of the conjugated C=O bond. This property was observed for catalysts with gold particle size <10 nm, however.

In addition, the support exerts a certain influence on the selectivity of gold. Milone et al. [2,3] suggested that an electron transfer from iron oxide support to gold particles creates electron-enriched gold particles on which the C=O bond is activated. Regarding crotonaldehyde hydrogenation, Bailie and Hutchings [5], working with Au/ZnO, Au/ZrO_2, and Au/SiO_2, found that the selectivity to crotyl alcohol depends on the nature of the support. For the same reaction, Okumura et al. [11] reported selectivity to crotyl alcohol ranging from 10 to 25% for Au/TiO_2, Au/Al_2O_3, and Au/SiO_2 catalysts. Because the gold particle size of these catalysts was in a similar range (3–5 nm), these authors concluded that the desired selectivity would be sensitive to the selection of the support. Schimpf et al. studied gold supported on SiO_2, TiO_2, and ZrO_2 [8] for the hydrogenation of acrolein and crotonaldehyde and reported a significant variation in selectivity (between 23 and 43%) for the different catalysts and they concluded that only the edges of crystallites are active sites for the preferred C=O hydrogenation. Because the support determines the morphology of the particles, its nature strongly influences the selectivity.

* Corresponding author.
E-mail address: mvolpe@plapiqui.edu.ar (M.A. Volpe).

0021-9517/$ – see front matter
doi:10.1016/j.jcat.2007.11.018

In a previous study, some of us [12] studied the hydrogenation of crotonaldehyde over gold supported on high-surface area ceria (240 $m^2\,g^{-1}$), Au/HSA–CeO_2. In that work, high selectivity toward the formation of crotyl alcohol was found. The gold particles were smaller than 4 nm, and the high selectivity value was considered an intrinsic property of gold nanoparticles. In addition, the redox properties of ceria promoted hydrogenation of the C=O bond. This effect was enhanced under certain pretreatment conditions, due to increased selectivity. However, the ceria acid–base characteristics gave rise to the formation of side products ethanol and condensation products.

Another important disadvantage of Au/HAS–CeO_2 is associated with the thermal instability of the support. Any treatment of this system at temperatures above 120 °C turns the catalyst inactive. In this context, it seems logical to study gold supported on ceria with surface area <240 $m^2\,g^{-1}$, over which side product formation would be diminished and thermal stability would increase.

In the present work, we studied gold supported on ceria with two different surface areas, 150 and 80 $m^2\,g^{-1}$, to further investigate the influence of the properties of ceria on the catalytic properties of gold for C=O activation.

2. Experimental

2.1. Catalyst preparation

Ceria with different surface areas were used as supports for gold, with 80 and 150 $m^2\,g^{-1}$, respectively. The former was obtained from the calcination of a ceria (Rhône Poulenc, Acalys HSA) with 240 $m^2\,g^{-1}$ surface area and 0.2 $ml\,g^{-1}$ pore volume at 800 °C for 8 h. The latter was a commercial ceria from Rhône Poulenc, with 150 $m^2\,g^{-1}$ surface area and 0.4 $ml\,g^{-1}$ pore volume.

The catalysts were prepared by the direct anionic-exchange method [13]. The support was dried in air at 500 °C and then mixed at 70 °C with an aqueous solution of $HAuCl_4{\cdot}xH_2O$ (Alfa Aesar) under vigorous stirring. The concentration of the gold precursor solution was fixed to obtain 2 wt% loaded catalysts. The suspension was washed with ammonia solution (4 $mol\,L^{-1}$) to eliminate Cl^- and then filtered and washed with water to eliminate ammonium species. The catalysts were then dried at 100 °C for 12 h and calcined under air at 300 °C (1 °C/min) for 4 h before being stored in a sealed vessel. The two catalysts are designated Au/$CeO_2$150 and Au/$CeO_2$80, respectively.

2.2. Catalyst characterization

The concentrations of gold and chlorine were determined using atomic absorption spectroscopy (AAS) at CNRS, Vernaison, France. BET surface areas of the supports and the catalysts were measured by N_2 physisorption at −196 °C with an automatic NOVA 1200e analyzer. Before each measurement, the samples were degassed for 1 h in helium at 100 °C. The catalysts were characterized by transmission electron microscopy (TEM) on a Jeol 100 CX2 (Tokyo, Japan) apparatus.

Catalyst reducibility was studied by temperature-programmed reduction (TPR) in a conventional flow system. Samples were previously calcined at 300 °C and then purged with Ar at the same temperature. Then the catalyst was cooled in Ar and switched to an H_2/Ar (5%) mixture. The temperature was increased linearly up to 900 °C, with hydrogen consumption monitored by a thermal conductivity detector.

X-ray diffraction (XRD) was used to estimate the gold particle size from Scherrer's analysis. XRD experiments were carried out on a D5000 Siemens diffractometer using Cu$K\alpha$ radiation ($\lambda = 0.15406$ nm). The scattering intensities were measured over an angular range of $15° < 2\theta < 65°$ for all the samples with a step size (2θ) of 0.02° and a step time of 2 s.

X-ray photoelectron spectroscopy (XPS) measurements were recorded on a VG-ESCA III spectrometer with Mg$K\alpha$ X-rays as photon source (1253.6 eV). Spectra were obtained for the C 1s, O 1s, Au 4f, and Ce 3d regions. For each case, the binding energy (BE) and the area of the corresponding peaks were measured. Due to the charging effect, the XPS peaks were found to shift toward higher BE. For this reason, C 1s BE (284.6 eV) was taken as an internal reference to correct peak position. For Au, 20 scans were accumulated for increasing the signal-to-noise ratio, whereas for Ce and C, 5 scans were accumulated. The Au/Ce atomic ratio was estimated by relating Au 4f (both peaks) and Ce 3d (all of the transitions in the corresponding region) areas after Shirley background subtraction and correction by mean scape depth and Scofield cross-section [14].

2.3. Catalytic test

The hydrogenation of crotonaldehyde was performed in a glass flow microreactor operating at atmospheric pressure, as described elsewhere [12]. Samples were submitted to two different in situ pretreatments: (a) reduction at 120, 300, and 500 °C for 1 h in H_2 and (b) calcination at 300 °C for 1 h with 25 $cm^3\,min^{-1}$ of air, cooling to room temperature, and reduction for 1 h at 120 °C. Between treatments, the reactor was exhaustively evacuated and purged with Ar.

The crotonaldehyde (Fluka puriss, 100–200 µl) was introduced in a trap, set before the reactor tube, and maintained at 0 °C to achieve constant crotonaldehyde partial pressure of 1.6 kPa. Two catharometers, inserted in the line at the input and output of the reactor, respectively, measure the reactant pressure throughout the experiment. When crotonaldehyde was injected, the reactor was kept closed, to avoid air contamination. Approximately 20 min later, the reactor was opened, after which the output signal immediately dropped to zero value. If no adsorption occurs on the catalyst, the output signal should recover to its initial level in about 30 s, the time it takes for gas to reach the catharometer.

The reaction products as well as the unreacted crotonaldehyde were analyzed at 10-min intervals online by a gas–liquid chromatograph equipped with a flame ionization detector (FID) and a 30-m-long, 0.5461-mm-diameter DB-Wax column (J&W Scientific). The condensation products were analyzed in a Chrompack CP-Wax-58CB column connected to a FISONS

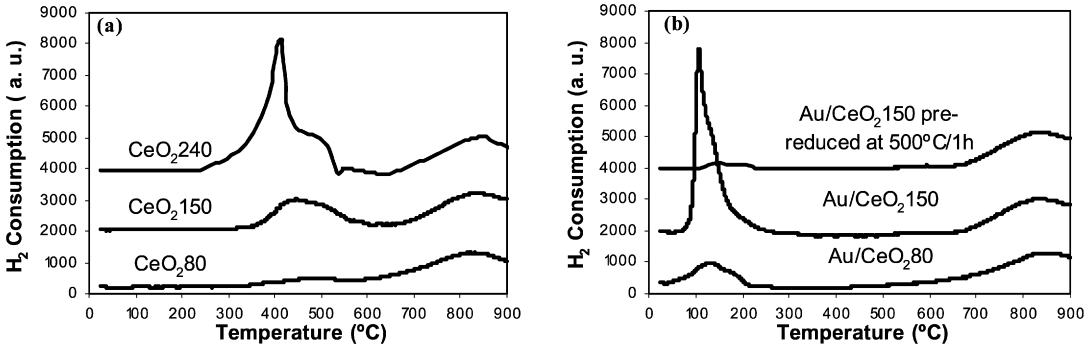

Fig. 1. (a) TPR on CeO_2 (240, 150, and 80 $m^2\,g^{-1}$), (b) $Au/CeO_2$80 and $Au/CeO_2$150 nonreduced and pre-reduced at 500 °C/1 h.

mass spectrometer, and the hydrocarbons using a chromatograph equipped with an FID and a CP-SIL5CB column. Further details of the analysis are available elsewhere [12].

The activity and selectivity toward the different products were measured, along with time on stream (TOS). The activity is reported in μmol converted per gram of catalyst per second ($\mu mol\,s^{-1}\,g^{-1}$). The selectivity was calculated as a ratio between a determined product and the sum of all products formed.

3. Results

3.1. Characterization

The gold content was approximately the same in the $Au/CeO_2$150 and $Au/CeO_2$80 catalysts (1.52 and 1.53 wt%, respectively) despite the difference in the specific surface area of the support. Almost all of the chlorine species were eliminated from the gold precursor, because the amount of Cl detected in the solids was <200 ppm.

TPR profiles corresponding to the $CeO_2$80 and $CeO_2$150 support (surface areas of 80 and 150 $m^2\,g^{-1}$, respectively) are shown in Fig. 1a. In both cases, two broad peaks of hydrogen consumption at 430 and 850 °C were observed. The lower of these is attributed to the surface reduction of O^{2-} and O^- anions attached to Ce^{4+} [15] and also to the reduction of surface Ce^{4+} to Ce^{3+}. The second peak (at 850 °C) is associated with reduction of the bulk oxygen and formation of lower-oxidation state cerium cations. The consumption associated with the $CeO_2$80 sample exhibited a smaller surface than that associated with the $CeO_2$150 support, due to the latter's higher specific area. For the sake of comparison, Fig. 1a also shows the profile corresponding to ceria with 240 $m^2\,g^{-1}$.

The TPR profiles of the $Au/CeO_2$80 and $Au/CeO_2$150 catalysts demonstrated the two characteristic peaks of ceria. For both samples, the first consumption peak was shifted to a lower temperature than in the bare support. This result was previously reported in previous work [12] and by other groups [16]. The low reduction peak (with maximum at 137 °C for $Au/CeO_2$80 and 106 °C for $Au/CeO_2$150) was larger for the catalyst with the higher surface area, as expected.

In other experiments, the $Au/CeO_2$150 and the $Au/CeO_2$80 samples were submitted to reduction at 500 °C before the usual TPR pretreatment. The profile corresponding the $Au/CeO_2$150 catalyst previously reduced at high temperature is shown in Fig. 1b. A strong diminished intensity of the low-temperature peak compared with the unreduced sample can be observed. Because the textural properties of the support were not modified by the reduction pretreatment (as measured by BET determination), the diminution of consumed hydrogen was related to depletion of the concentration gold–ceria interphase sites due to gold particle sintering. The same trends were observed for the $Au/CeO_2$150 catalyst. This result suggests that gold crystallites undergo a sintering process after reduction at high temperature.

We attempted to determine the mean particle size for the Au/CeO_2 samples, because this feature plays an important role in determining the catalytic pattern in the hydrogenation of α, β-unsaturated aldehydes [5,10]. First, we conducted a TEM study for the $Au/CeO_2$80. Although the contrast between the support and the gold particles was rather low, the observation of some crystals on a micrograph allowed us to estimate a metal crystallite size of 9 nm. Moreover, to study the dependence of gold particle size on the reduction pretreatment temperature, we compared TEM results corresponding to the $Au/CeO_2$80 sample for the sample reduced at 120 and 500 °C. The particle sizes ranged from 9 to 15 nm with increasing reduction temperature.

For the $Au/CeO_2$150 sample, TEM images showed a very small contrast between gold and ceria, as was reported previously for the high-surface area catalyst, $Au/CeO_2$240 [12]. Haruta et al. failed to observe Au nanoparticles supported on CeO_2 by TEM [17]; however, in this case the support area (not reported by the authors) likely was relatively low, considering that the study was carried out over a model catalyst.

Taking into account that no clear morphologic characterization was obtained for the $Au/CeO_2$150 catalyst by TEM, we performed an XRD analysis of the samples thus formed. Table 1 reports the results corresponding to gold particle size obtained from Scherrer's analysis of the XRD main gold diffraction peak (111 plane). It can be seen that gold crystals were relatively large for both low- and medium-surface area catalysts (11 and 10 nm, respectively).

We performed an XPS study to investigate the possible sintering of gold particles submitted to reduction treatment at high temperature. The 4f XPS peaks of Au on the $Au/CeO_2$80 and $Au/CeO_2$150 catalysts are shown in Fig. 2. From the corrected relation of the area of these peaks and those corresponding to Ce 3d, we calculated the Au/Ce atomic ratio; these ratios are reported in Table 1. A decrease in these values with increasing reduction temperature can be seen, demonstrating unambigu-

Table 1
Physicochemical properties of Au/CeO_2 catalysts reduced at 120 and at 500 °C

Sample	Gold content (wt%)	Particle size (nm)	BET surface area ($m^2\ g^{-1}$)	Au/Ce[c]
$Au/CeO_2$80 Red. 120 °C	1.52	9[a]–11[b]	80	0.32
$Au/CeO_2$80 Red. 500 °C		15[a]	80	0.26
$Au/CeO_2$150 Red. 120 °C	1.53	10[b]	150	0.20
$Au/CeO_2$150 Red. 500 °C			150	0.18

[a] Particle size obtained from TEM.
[b] Particle size obtained from Scherrer's analysis of XRD data.
[c] Atomic ratio as measured by XPS.

ously that sintering of gold particles with temperature occurred for both samples, in agreement with the TPR and TEM results for samples prereduced at high temperatures.

Although the BE of gold peaks can be measured from the data given in Fig. 2, the analysis of the chemical state of gold in the present samples is beyond the scope of the present contribution.

3.2. Catalytic results

3.2.1. Crotonaldehyde hydrogenation on bare ceria

No significant activity was observed on the bare supports. However, for both low- and medium-surface area ceria, an extended adsorption of the crotonaldehyde was detected. This period was shorter for $CeO_2$80 (5 min) than for $CeO_2$150 (10 min).

3.2.2. Crotonaldehyde hydrogenation on $Au/CeO_2$80 and $Au/CeO_2$150 at 120 °C, pretreatment **a**: reduction for 1 h at 120 °C under H_2

Figs. 3a and 3b report the dependence of conversion and of the selectivity to different products on TOS for the $Au/CeO_2$80 and $Au/CeO_2$150 catalysts respectively. Both samples demonstrate a deactivation stage during which the product distributions strongly varied with TOS. In the first of these, the main product in both cases was ethanol (EOL), although in the case of $Au/CeO_2$150, its production was much higher than for $Au/CeO_2$80 (85 and 44 $\times\ 10^{-8}$ mol s^{-1} g_{cat}^{-1}, respectively). Crotyl alcohol (UOL), butanal (BAL), and butanol (BOL) were also detected, whereas C4 hydrocarbons were produced in minor amounts.

Afterward, a quasi-steady state was reached. Ethanol almost disappeared at the start of this period, at the same time that condensation products (CPs) appeared. The main CP was 2-, 4-, 6-octatrienal, as identified by mass spectrometry. This fact suggests that both CP and UOL were formed over the same sites.

For both samples, in the steady-state phase, crotyl alcohol deceased with TOS while butanal increased, becoming the main product. This indicates that the samples turn into rather unselective catalysts under reaction conditions. The selectivity to UOL and the yield to this product and the crotyl alcohol-to-butanal ratio are reported in Table 1. Though catalytic trends corresponding to the $Au/CeO_2$80 catalysts were similar to those of the $Au/CeO_2$150 sample, all these parameters in the steady state phase was lower for the former than for the latter catalysts. Thus, $Au/CeO_2$150 is considered to be more selective than $Au/CeO_2$80.

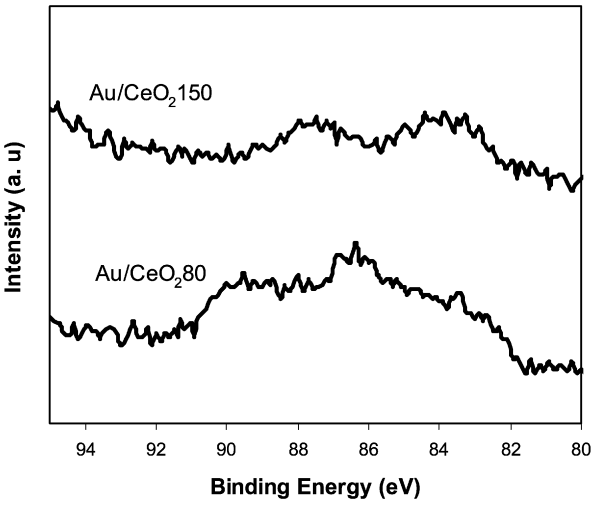

Fig. 2. XPS analysis: Au 4f in $Au/CeO_2$150 and $Au/CeO_2$80.

3.2.3. Crotonaldehyde hydrogenation on $Au/CeO_2$80 and $AuCeO_2$150 at 120 °C, pretreatment **b**

Based on previous results [12] indicating a strong beneficial effect of calcination pretreatment on the yield toward crotyl alcohol of $Au/CeO_2$240, we submitted the $Au/CeO_2$80 and $Au/CeO_2$150 samples to pretreatment **b**. The initial yields to ethanol are strongly influenced by the pretreatment; ethanol production in the samples submitted to pretreament **a** was higher than that in the samples submitted to pretreatment **b**. The initial yields to ethanol (during the deactivation period) were 70 and 17 $\times\ 10^{-8}$ mol s^{-1} g_{cat}^{-1} (see Table 2) for the medium- and the low-surface area catalysts, respectively.

Regarding the steady-state regime, Fig. 4 compare the yields to the different products for the $Au/CeO_2$80 catalyst corresponding to pretreatments **a** and **b**. The activity corresponding to pretreatment **b** was higher than that for pretreatment **a**. The yield to CP was negligible for both pretreatments. The same catalytic trends were observed for $Au/CeO_2$150. For this catalyst, the production of CP for pretreatment **b** was null, whereas a yield of 0.2 $\times\ 10^{-8}$ mol s^{-1} g_{cat}^{-1} was measured over the same sample submitted to pretreatment **a**.

On a steady-state regime, slightly higher crotyl alcohol production was detected after calcinations pretreatment for the $Au/CeO_2$150 catalyst, whereas no enhancement of the production of the desired product was detected for the low-surface area sample. Table 1 reports the selectivity to crotyl alcohol, as well as the crotyl alcohol-to-butanal ratio, indicating less improvement than was found for the $Au/CeO_2$240 sample [12].

3.2.4. Crotonaldehyde hydrogenation on $Au/CeO_2$80 and Au/CeO_2: Influence of the temperature of the reduction pretreatment

The temperature of the reduction pretreatment was increased in an attempt to create more Ce^{3+} species or induce an in-

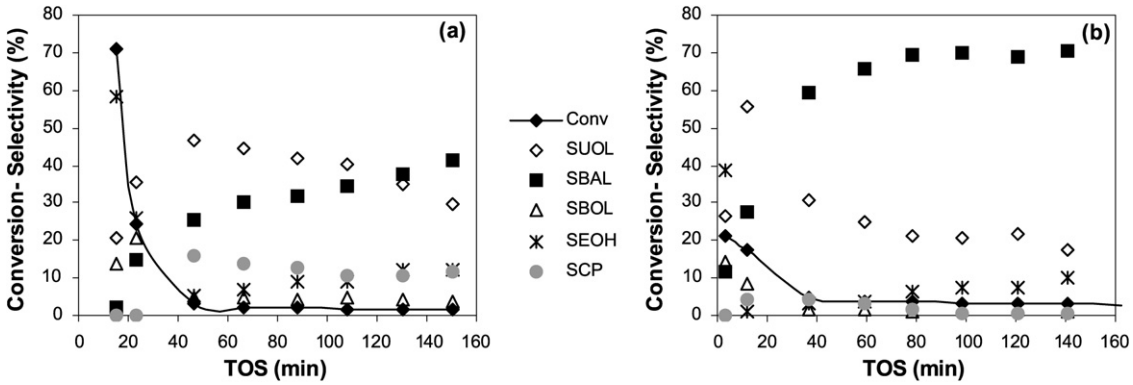

Fig. 3. Crotonaldehyde hydrogenation on (a) Au/$CeO_2$150 and (b) Au/$CeO_2$80. Samples reduced 1 h at 120 °C, reaction temperature 120 °C. Dependence of activity and selectivity to different products on TOS.

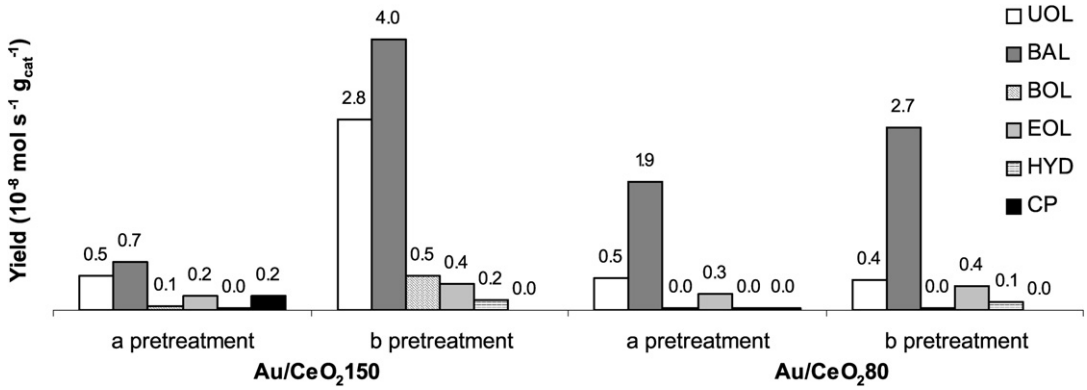

Fig. 4. Crotonaldehyde hydrogenation on (a) Au/$CeO_2$150 and (b) Au/$CeO_2$80. Samples reduced at 120 °C, reaction temperature 120 °C. Yield to the different products corresponding to **a** and **b** pre-treatments at steady state regime.

Table 2
Hydrogenation of crotonaldehyde[a]

Sample	Initial total yield[b]		Initial yield to ethanol[c]
	a pre-treatment	**b** pre-treatment	
Au/$CeO_2$80 120 °C	0.17	0.45	6.1
Au/$CeO_2$80 500 °C		0.11	0.3
Au/$CeO_2$150 120 °C	0.73	0.81	4.8
Au/$CeO_2$150 500 °C		0.08	0.2

[a] Samples reduced at 120 °C in hydrogen.
[b] 10^{-7} mol s^{-1} g_{cat}^{-1} measured at 10 min TOS. Deactivation period.
[c] 10^{-8} mol s^{-1} g_{cat}^{-1}, **b** pre-treatment.

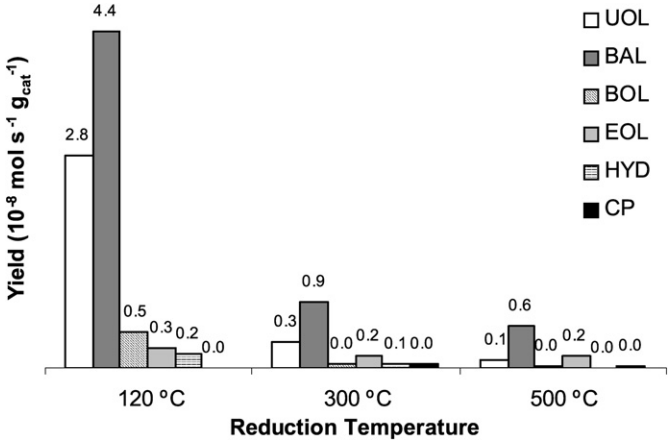

Fig. 5. Crotonaldehyde hydrogenation on Au/$CeO_2$150. Sample pre-reduced at 120, 300 and 500 °C. Yields to different products under steady state regime.

teraction between the gold and the support. The deactivation period observed previously was not detected for the catalysts prereduced at 500 °C; that is, the conversion was nearly constant throughout the TOS. Moreover, the activity attained under the steady-state regime was strongly dependent on the temperature of the reduction pretreatment; the higher the temperature of the reduction pretreatment, the lower the activity of the sample. Fig. 5 shows the yields to the different products (butanal, butanol, crotyl alcohol, and condensation products) corresponding to the Au/$CeO_2$80 and Au/$CeO_2$150 catalysts under the steady-state regime for the different temperatures of reduction pretreatment. As shown, the dependence product distribution was not greatly influenced by the prereduction temperature.

3.2.5. *Crotonaldehyde hydrogenation: Effect of the reaction temperature (samples reduced at 120 °C, pretreatment **a**)*

Fig. 6 reports the yields to each product in the steady-state phase over Au/$CeO_2$150 for reaction temperatures of 120, 150, and 180 °C. The increase in reaction temperature caused an in-

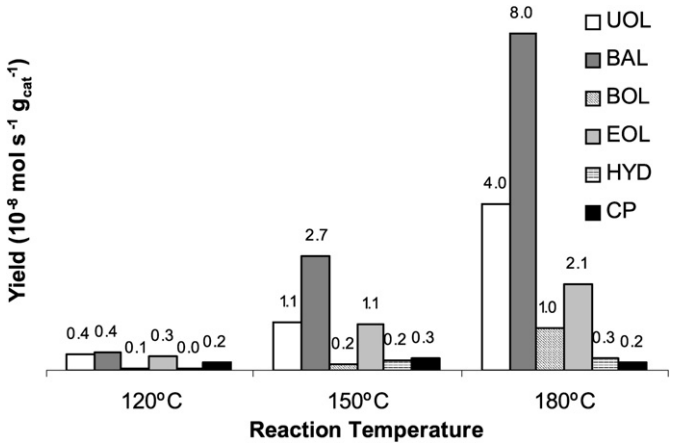

Fig. 6. Crotonaldehyde hydrogenation on Au/$CeO_2$150 and Au/$CeO_2$80. Samples reduced at 120, reaction temperatures 120, 150, and 180 °C. Yields to the different product under steady state regime.

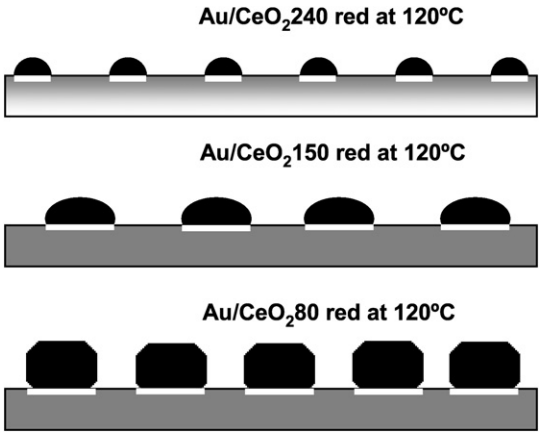

Fig. 7. Model of gold particles in Au/$CeO_2$80, Au/$CeO_2$150, and Au/$CeO_2$240.

crease in the yields to crotyl alcohol and butanal but a decrease in condentation products. The formation of butanal was favored over that of crotyl alcohol, due to the differing activation energies for the hydrogenation of the olefinic and carbonyl bonds (30.8 and 42.3 kJ/mol^{-1}, respectively).

4. Discussion

Here we compare the results of the present work on gold supported on ceria with low and medium surface areas (80 and 150 m^2 g^{-1}, respectively), with previously reported results for gold supported on high-surface area ceria, Au/$CeO_2$240 [12] and discuss the catalytic and characterization results. Regardless of the specific surface area of the support (80, 150, or 240 m^2/g), the loading of gold fixed by the solid remains almost the same (1.5–1.8 wt%). To explain this fact, it could be argued that during the impregnation step, the acid pH of the precursor solution modifies the support surface in all the cases, creating a similar concentration of acid Lewis sites (cationic vacancies) responsible for the anchoring the metal.

Based on TPR results, we determined that the concentration of surface oxygen anions and reducible ceria species were (as expected) lower on low-surface area ceria than on medium-surface area ceria. Because these species are stabilized on nucleated oxygen vacancies on the ceria surface [18,19], TPR can account for a dependence of the vacancy concentration on the surface area of ceria. Wahlström et al. [20] postulated that oxygen vacancies are active nucleation sites for Au clusters on rutile surface, whereas Lai and co-workers [21], based on FTIR of adsorbed CO results, indicated that low-coordination ceria sites in association with oxygen vacancy sites are responsible for the strong binding of small gold particles. One could argue that high-surface area ceria can stabilize gold at high dispersion. This would be in line with the fact that gold particles are relatively large on low- and medium-surface area ceria (as measured by TEM and XRD analysis) but are <4 nm for high-surface area ceria (as deduced from XRD analysis in Ref. [12]). Furthermore, the different surface area of the supports also would play a role in the resistance of gold particles to sintering. Nanogold structures supported on high-surface area ceria particles had a high resistance to sintering, with the opposite occurring for Au/$CeO_2$80 and Au/$CeO_2$150, as the TPR and XPS results clearly showed. This would account for the fact that after these samples were reduced at high temperature, the gold particle size increased from 9 to 15 nm for Au/$CeO_2$80. The entire scenario is depicted in the scheme shown in Fig. 7.

Regarding the hydrogenation of crotonaldehyde over Au/$CeO_2$80 and Au/$CeO_2$150 performed at 120 °C, the catalysts demonstrated strong deactivation with TOS. No C3 hydrocarbons were detected over all of the TOS studied; thus, deactivation due to decarbonylation reaction producing strong CO adsorption of metal surface is disregarded. It can be speculated that catalyst decay resulted from the formation of coke deposits produced from dienic polymers originating from adsorbed crotonaldehyde.

The main product of the deactivation period was ethanol, formed following a reaction postulated in a previous study [12],

$$\begin{aligned} CH_3\text{–}CH{=}CH\text{–}CHO &\rightarrow CH_3\text{–}CHOH\text{–}CH_2\text{–}CHO \\ &\rightarrow 2CH_3\text{–}CH_2OH. \end{aligned} \quad (1)$$

The first step, hydration of the C=C bond, occurs on ceria sites, consuming surface OH groups. In the second step, hydrogenolysis of the C(2)–C(3) bond, hydrogen atoms coming from dissociated H_2 on the metallic gold particles participate. Considering that H_2 chemisorption occurs on surface atoms of low coordination number [22], reaction (1) would occur on highly dispersed gold. Both active sites are necessary for the formation of ethanol and OH from the support and metallic gold particles. This explains why the yield of ethanol depends on the specific surface area of the support, as well as on the gold particle size. The yield for the medium-surface area catalyst (Au/$CeO_2$150) was higher that that of the low-surface area catalyst (Au/$CeO_2$80), due to the former's larger specific surface area and smaller particle size. Au/$CeO_2$240, with a high concentration of both active sites due to its high surface and the relatively small particle size, exhibited high initial activity for ethanol formation.

It was previously postulated [12] that the formation of ethanol results in iginates Lewis acid sites. In a second step,

these Lewis center are the active sites for the formation of condensation products (see reaction (3) in Ref. [12]). For this reason, the higher the production of ethanol in the initial state, the higher the production of CP under the steady-state regime. In line with this, the yield to CP was higher for Au/CeO_2150 (initial yield to ethanol, 85×10^{-8} mol s^{-1} g_{cat}^{-1}) than for $Au/CeO_2 80$ (initial yield to ethanol, 44×10^{-8} mol s^{-1} g_{cat}^{-1}).

In previous work [12], it was concluded that pretreatment **b** leads to a diminished number of OH groups on the ceria surface and concomitantly a diminished yield to ethanol. In the samples studied in the present work, the initial yield of ethanol was lower for pretreatment **a** than for pretreatment **b**.

For previously studied Au/CeO_2240, the decreased formation of condensation products led to an increase in the yield of crotyl alcohol in the steady-state regime. The improved selectivity was due to an increase in the availability of the sites responsible for formation of condensation products: surface oxygen vacancies, V_O^0. In turn, the formation of Ce^{3+} centers also increased, following:

$$V_O^0 + Ce^{4+} \rightleftarrows Ce^{3+} + e^-. \quad (2)$$

The formation of crotyl alcohol was higher when the equilibrium (2) was displaced to the right, due to a promotional effect of Ce^{3+} cations. In this way, the low- and medium-surface area ceria, showing meager production of the secondary products, would give rise to a highly selective catalyst. However, the expected increase in selectivity was not observed for the low- and medium-surface area catalysts; the selectivity to crotyl alcohol was approximately 10% for $Au/CeO_2 80$ versus 63% for Au/CeO_2240 (steady-state values, for samples submitted to pretreatment **a**). It could be speculated that the concentration of V_O^0 sites of the low-surface area support was not sufficient to produce Ce^{3+} sites following reaction (2). Concomitantly, no promotional effect of the support occurred in the low-surface area ceria.

The selectivities to crotyl alcohol for the $Au/CeO_2 80$ catalyst under different reaction and pretreatment conditions were similar to the values reported by other groups for Au supported on "inert" supports. For example, Haruta et al. [11] found a selectivity to crotyl alcohol of 10% for an alumina-supported catalyst. The selectivity corresponding to the Au/CeO_2150 sample was higher (30–33%) than that corresponding to the $Au/CeO_2 80$ catalyst. The difference in selectivity to the desired product between these samples is related to the fact that the V_O^0 concentration for the CeO_2150 was higher than that of the $CeO_2 80$.

At this point, the different catalytic results have been discussed based mainly on the different surface areas of the supports. However, the role of particle size should be considered for the present catalysts with a relatively large particle size (9–11 nm). Bailie and Hutchings [5], studying Au/ZnO, Au/ZrO_2, and Au/SiO_2, suggested that high activity and selectivity of Au catalysts are associated with small particles. An effect of particle size on selectivity toward hydrogenation of the C=O bond also would explain the difference between the samples that we studied and the high-surface area catalyst. Furthermore, the diminished selectivity toward crotyl alcohol with increasing prereduction temperature would be related to an enlargement of crystallites after high-temperature reduction. This particle size modification was clearly demonstrated by the XPS and TPR experiments. A decreased specific surface area was ruled out based on BET analysis of the samples reduced at high temperature.

In steady-state conditions at 120 °C, $Au/CeO_2 80$ and Au/CeO_2150 have lower activity than Au/CeO_2240. The difference in the activity between high- and low-surface area samples can be ascribed to a size effect; the gold particles on the low-surface area ceria catalyst were larger than those supported on the high-surface area ceria catalyst, but are rather inactive toward hydrogenation reactions.

5. Conclusion

The supports used in this work (with surface areas of 150 and 80 $m^2\,g^{-1}$) should not be considered convenient materials for gold, because the catalysts present relatively low activity and selectivity to crotyl alcohol in the hydrogenation of crotonaldehyde at atmospheric pressure. This occurs because (i) the concentration of surface sites of the support responsible for a promotional effect on gold catalytic properties are too low, and thus no increase of gold selectivity can be achieved due to the support, and (ii) gold particles are relatively large and quite unstable under reaction conditions. Comparing the present results with those corresponding to Au supported on high-surface area ceria (240 $m^2\,g^{-1}$) indicates that the latter support leads to highly selective catalyst in which ceria redox and acid-base properties are engaged in a promotional effect.

Acknowledgments

The authors thank Svetlana Ivanova and Raymonde Touroude for fruitful discussions.

References

[1] M.A. Vannice, B. Sen, J. Catal. 115 (1989) 65.
[2] C. Milone, R. Ingoglia, A. Pistone, G. Neri, F. Frusteri, S.J. Galvagno, J. Catal. 222 (2004) 348.
[3] C. Milone, R. Ingoglia, L. Schipilliti, C. Crisafulli, G. Neri, S. Galvagno, J. Catal. 236 (2005) 80.
[4] J.E. Bailie, G.J. Hutchings, Catal. Commun. 2 (2001) 29.
[5] J.E. Bailie, G.J. Hutchings, Chem. Commun. (1999) 2151.
[6] M. Shibata, N. Kawata, T. Masumuto, H. Kimura, J. Chem. Soc. Chem. Commun. (1988) 154.
[7] C. Mohr, P. Claus, Sci. Prog. 84 (4) (2001) 311.
[8] S. Schimpf, M. Lucas, C. Mohr, U. Rodemerck, A. Brückner, J. Radnik, H. Hofmeister, P. Claus, Catal. Today 72 (2002) 63.
[9] P. Claus, Appl. Catal. A. Gen. 291 (2005) 222.
[10] R. Zanella, C. Louis, S. Giorgio, R. Touroude, J. Catal. 223 (2004) 328.
[11] M. Okumura, T. Akita, M. Haruta, Catal. Today 2688 (2002) 1.
[12] B. Campo, M. Volpe, S. Ivanova, R. Touroude, J. Catal. 242 (2006) 162.
[13] S. Ivanova, V. Pitchon, Y. Zimmermann, C. Petit, App. Catal. A Gen. 298 (2006) 57.
[14] J.H. Scofield, J. Electron. Spectrosc. Relat. Phenom. 8 (1976) 29.
[15] S. Scirè, S. Minicò, C. Crisafulli, C. Satriano, A. Pistone, Appl. Catal. B Environ. 40 (2003) 43.
[16] D. Andreeva, V. Idakiev, T. Tabakova, L. Ilieva, P. Falaras, A. Bourlinos, A. Travlos, Catal. Today 72 (2002) 51.

[17] T. Akita, M. Okumura, K. Tanaka, M. Kohyama, M. Haruta, Catal. Today 117 (2006) 62.
[18] Q. Fu, H. Saltsburg, M. Flytzani-Stephanopoulos, Science 301 (2003) 935.
[19] Q. Fu, W. Deng, H. Saltsburg, M. Flytzani-Stephanopoulos, Appl. Catal. B Environ. 56 (2005) 57.
[20] E. Wahlström, N. Lopez, R. Schaub, P. Thostrup, A. Rønnau, C. Africh, E. Lagsgaard, J. Nørskov, F. Besenbaches, Phys. Rev. Lett. 90 (2003) 026101.
[21] S.-Y. Lai, Y. Qiu, S. Wang, J. Catal. 237 (2006) 303.
[22] L. Stobinsky, L. Zommer, R. Dus, Appl. Surf. Sci. 141 (1999) 319.